Economic Model Predictive Control of Nonlinear Process Systems Using Empirical Models

Anas Alanqar and Matthew Ellis
Dept. of Chemical and Biomolecular Engineering, University of California, Los Angeles, CA 90095

Panagiotis D. Christofides
Dept. of Chemical and Biomolecular Engineering, University of California, Los Angeles, CA 90095

Dept. of Electrical Engineering, University of California, Los Angeles, CA 90095

DOI 10.1002/aic.14683
Published online November 28, 2014 in Wiley Online Library (wileyonlinelibrary.com)

Economic model predictive control (EMPC) is a feedback control technique that attempts to tightly integrate economic optimization and feedback control since it is a predictive control scheme that is formulated with an objective function representing the process economics. As its name implies, EMPC requires the availability of a dynamic model to compute its control actions and such a model may be obtained either through application of first principles or through system identification techniques. In industrial practice, it may be difficult in general to obtain an accurate first-principles model of the process. Motivated by this, in the present work, Lyapunov-based EMPC (LEMPC) is designed with a linear empirical model that allows for closed-loop stability guarantees in the context of nonlinear chemical processes. Specifically, when the linear model provides a sufficient degree of accuracy in the region where time varying economically optimal operation is considered, conditions for closed-loop stability under the LEMPC scheme based on the empirical model are derived. The LEMPC scheme is applied to a chemical process example to demonstrate its closed-loop stability and performance properties as well as significant computational advantages. © 2014 American Institute of Chemical Engineers *AIChE J*, 61: 816–830, 2015

Keywords: economic model predictive control, system identification, process control, process optimization, process economics, chemical processes

Introduction

The economic success of the chemical and petrochemical industry relies on optimal process operation which has led to the emergence of an overall process control goal of translating process/system economic considerations into feedback control objectives.[1] One key development toward achieving this goal is economic model predictive control (EMPC). EMPC is a feedback control technique that attempts to tightly integrate economic optimization and feedback control since it is a predictive control scheme that is formulated with an objective function representing the process/system economics[2–4] (see, also, Ref. 5 for an overview of recent results on EMPC). While initial efforts on EMPC have focused on closed-loop stability considerations, recent developments have addressed economic performance including: formulating a Lyapunov-based EMPC with guaranteed closed-loop economic performance improvement over conventional (tracking) model predictive control (MPC) over finite-time and infinite-time operating intervals,[6] investigating the transient performance and closed-loop stability of EMPC formulated without terminal constraints,[7] and studying the closed-loop performance of EMPC formulated with a self-tuning terminal cost and generalized terminal constraint.[8]

The key underlying assumption to design and apply an EMPC is that a process/system dynamic model is available to predict the future process state evolution. Constructing models of dynamical systems is done either through first principles and/or from process input/output data.[9] First-principle models are developed from conservation equations and attempt to account for the essential mechanisms behind the observed physicochemical phenomena. However, arriving at a first-principles model requires sufficient process knowledge which may be a challenging task for complex industrial processes. On the other hand, system identification serves as an alternative to first-principles models when first-principles models are unavailable and/or too complex to use on-line in MPC. Over the past 30 years, numerous methods have been developed to construct linear or nonlinear empirical models from input/output data (see, for example, Refs. 10–14 and the references contained therein for an overview of these methods). One potential grouping of the various methods of system identification is to group the methods on the basis of the type of empirical model derived which may be either an input-output model or a state-space model. However, note that when the output vector is the entire state vector (i.e., full-state feedback), input-output modeling methods may be used to construct a state-space model. The most common

Correspondence concerning this article should be addressed to P. D. Christofides at pdc@seas.ucla.edu.

type of empirical model is a linear model. When a process system exhibits significant nonlinearities as is the case in most chemical processes, the use of multiple linear models has been employed to improve the accuracy of prediction over a larger operating region.[15–17]

Within the context of input-output models, (nonlinear) autoregressive moving average with exogenous input models ((N)ARMAX), Volterra models, and neural-network models are some of the types of input-output models commonly used (see, for instance, Refs. 13,14 and the references therein for more details on input-output modeling). Numerous works on integrating input-output models within the context of tracking MPC, which is formulated with a cost function that is positive definite with respect to a set-point or steady-state, have been investigated. For instance, the use of Hammerstein, Wiener, and Hammerstein-Wiener models within MPC[18–20] has been considered, the use of multiple-models within MPC constructed from autoregressive with exogenous input (ARX) models has been investigated for batch processes (e.g., Ref. 21), and multiple-model adaptive predictive control has been formulated for mean arterial pressure and cardiac output regulation (e.g., Ref. 22).

On the other hand, empirical state-space modeling methods are another type of empirical modeling technique. Within this context, linear subspace system identification is a very widely known and used empirical modeling method that is based on input/output data.[23–29] In particular, subspace model identification (SMI) methods are noniterative methods that take into account multivariable interactions and result in models that are numerically stable for multiple-input multiple-output (MIMO) systems.[25,29,30] Some of the various SMI algorithms in the literature include the multivariable output error state-space algorithm (MOESP),[23,24,26,31] the Canonical Variate Algorithm (CVA),[32] and numerical algorithms for subspace state-space system identification (N4SID).[25] Identifying the deterministic part of a MIMO state-space model using SMI methods has proven to be successful in the context of industrial settings.[24,31,33–35] Combining subspace methods with MPC has also been considered (see, for instance, Ref. 28 and the references contained therein).

To date, no work on formulating an EMPC scheme using an empirical model with guaranteed closed-loop stability properties has been completed. In this work, an integrated view of system modeling, feedback control, and process/system economics is undertaken. Specifically, an LEMPC formulated with an empirical model is considered. The type of empirical model is restricted to state-space models given the fact that the economic cost function typically depends on at least some (if not all) of the state variables. While the linear model may be derived from any system identification technique, it must be sufficiently close (in a sense to be made precise below) to the linearization of the nonlinear process model at the steady-state around which time-varying operation is considered. Under this assumption, sufficient conditions for closed-loop stability (boundedness of the closed-loop state in a compact state-space set) under the LEMPC with the empirical linear model applied to the nonlinear chemical process are derived. The LEMPC with empirical model method is applied to a chemical process example and extensive closed-loop simulations are performed that demonstrate the closed-loop stability and performance properties. Furthermore, a significant reduction in the on-line computation time with LEMPC formulated with an empirical model is realized over LEMPC formulated with a nonlinear first-principles model.

Preliminaries

Notation

The Euclidean norm of a vector is denoted by the operator $|\cdot|$ and the norm of a matrix is denoted as $||\cdot||$. A continuous function $\alpha : [0, a) \to [0, \infty)$ is said to belong to class $\mathcal{K}$ if it is strictly increasing and is zero when evaluated at zero. The symbol Ω_ρ is used to denote the set $\Omega_\rho := \{x \in R^n : V(x) \le \rho\}$ where V is a continuously differentiable positive definite scalar function and $\rho > 0$, and the symbol $S(\Delta)$ denotes the family of piecewise constant functions with period Δ. The transpose of the vector x is denoted x^T.

Class of systems

The class of nonlinear process systems considered can be written in the following continuous-time state-space form

$$\dot{x}(t) = f(x(t), u(t), w(t)) \tag{1}$$

where $x \in R^n$ is the state vector of the system, $u \in R^m$ is the control (manipulated) input vector, and $w \in R^l$ is the disturbance vector. The vector function $f(\cdot,\cdot,\cdot)$ is assumed to be a locally Lipschitz vector function. The control actions are bounded by the physical constraints on the control actuators and thus, are restricted to belong to a nonempty convex set $U := \{u \in R^m : u_i^{\min} \le u_i \le u_i^{\max},\ i = 1, \ldots, m\}$. The norm of the disturbance vector is bounded (i.e. $|w(t)| \le \theta$ for all t where $\theta > 0$ bounds the norm). The equilibrium of the system of Eq. 1 is considered to be the origin, i.e., $f(0, 0, 0) = 0$. The state of the system of Eq. 1 is assumed to be synchronously sampled and available at sampling time instances $t_k := k\Delta$, $k = 0, 1, \ldots$where $\Delta > 0$ is the sampling period.

We restrict the class of nonlinear systems of Eq. 1 considered to a class of stabilizable nonlinear systems. Specifically, we assume the existence of a Lyapunov-based controller $h(x) \in U$ that renders the origin of the closed-loop nominal system ($w(t) \equiv 0$) of Eq. 1 asymptotically stable for all x in an open neighborhood of the origin. This assumption implies the existence of a continuously differentiable Lyapunov function, $V : R^n \to R_+$, for the closed-loop system of Eq. 1 under $u(t) = h(x(t))$ that satisfies[36,37]

$$\alpha_1(|x|) \le V(x) \le \alpha_2(|x|), \tag{2a}$$

$$\frac{\partial V(x)}{\partial x} f(x, h(x), 0) \le -\alpha_3(|x|), \tag{2b}$$

$$\left|\frac{\partial V(x)}{\partial x}\right| \le \alpha_4(|x|) \tag{2c}$$

for all $x \in D \subseteq R^{n_x}$ where D is an open neighborhood of the origin and $\alpha_i(\cdot)$, $i = 1, 2, 3, 4$ are functions of class $\mathcal{K}$. For various classes of nonlinear systems, stabilizing control laws that explicitly account for input constraints have been developed (see, for example, Refs. 38–41 for results in this direction). The stability region (i.e., the set of points in state-space where convergence to the origin under the Lyapunov-based controller is guaranteed) may be estimated as the level set of the Lyapunov function where the time-derivative of the Lyapunov function is negative for all points contained in the level set, and is denoted as $\Omega_\rho \subset D$. Moreover, the origin of the sampled-data system resulting from the system of Eq. 1 under the Lyapunov-based controller when implemented in a sample-and-hold fashion is practically stable (i.e., the closed-loop state will converge to a small compact, forward invariant set containing the origin in its interior) when a

sufficiently small sampling period is used and the bound on the disturbance vector is sufficiently small.[42]

In this work, empirical models will be constructed to predict the evolution of the state of the system of Eq. 1 using data-based modeling techniques. Specifically, the type of empirical models constructed for the system of Eq. 1 are linear time-invariant state-space models which have the following form

$$\dot{x}(t)=Ax(t)+Bu(t) \tag{3}$$

where $x \in R^n$ is the state vector, $u \in R^m$ is the input vector, and A and B are constant matrices of appropriate dimensions. When the nominal nonlinear model of Eq. 1 is unavailable, the Lyapunov-based controller needs to be designed on the basis of the empirical model of Eq. 3. We assume that the pair (A, B) is stabilizable in the sense that there exists a state feedback controller $h_L(x) \in U$ that renders the origin of the closed-loop system of Eq. 3 exponentially stable for all initial conditions $x \in D_L$ where D_L is some open neighborhood of the origin. Furthermore, the controller $h_L(x) \in U$ is assumed to be locally Lipschitz on R^n in the sense that there exists a $K>0$ such that $|h_L(x)|$ can be bounded by $K|x|$ for all x in a compact set containing the origin in its interior. When the controller $h_L(x)$ is applied to the nominal nonlinear system of Eq. 1, there are two factors that affect closed-loop stability: the closeness of the model of Eq. 3 to the linearization of the nominal model of Eq. 1 at the origin and the effect of the nonlinearities of the system of Eq. 1. Locally, we can show that the controller $h_L(x)$ possesses a robustness margin to overcome these two effects and render the origin of the nominal closed-loop nonlinear system asymptotically stable. This is stated in the following proposition.

Proposition 1. *If the origin of closed-loop system of Eq. 3 under the controller $h_L(x)$ is exponentially stable and there exist $\hat{\rho} > 0$ and $\delta > 0$ such that*

$$||\bar{A}-A||+||\bar{B}-B||K \leq \delta \tag{4}$$

where the matrices $\bar{A}$ and $\bar{B}$ denote the linearization of f(x, u, 0) at the origin

$$\bar{A} := \frac{\partial f}{\partial x}(0,0,0), \quad \bar{B} := \frac{\partial f}{\partial u}(0,0,0) \tag{5}$$

then the origin of the nominal closed-loop system of Eq. 1 ($w(t) \equiv 0$) is exponentially stable for all $x \in \Omega_{\hat{\rho}} \subset D_L$.

Proof. To prove the result of Proposition 1, we will show that there exists a Lyapunov function for the closed-loop system of Eq. 1 under the controller $h_L(x)$ when $\hat{\rho} > 0$ and $\delta > 0$ are sufficiently small. Owing to the fact that the origin of closed-loop system of Eq. 3 under the controller $h_L(x)$ is exponentially stable, there exists a continuously differentiable Lyapunov function $\hat{V} : R^n \rightarrow R_+$ such that[37]

$$c_1|x|^2 \leq \hat{V}(x) \leq c_2|x|^2, \tag{6a}$$

$$\frac{\partial \hat{V}(x)}{\partial x}(Ax+Bh_L(x)) \leq -c_3|x|^2, \tag{6b}$$

$$\left|\frac{\partial \hat{V}(x)}{\partial x}\right| \leq c_4|x| \tag{6c}$$

for all $x \in D_L$ where c_i, $i = 1, 2, 3, 4$ are positive constants. Define

$$g(x) := f(x, h_L(x), 0)-\bar{A}x-\bar{B}h_L(x) \tag{7}$$

which contains terms of second-order and higher in x. Consider the following closed-loop system

$$\dot{x}=Ax+Bh_L(x)+f(x, h_L(x), 0)-Ax-Bh_L(x) \tag{8}$$

and the time-derivative of $\hat{V}$ along the trajectory of the closed-loop system of Eq. 8

$$\begin{aligned}\dot{\hat{V}} &= \frac{\partial \hat{V}(x)}{\partial x}(Ax+Bh_L(x))+\frac{\partial \hat{V}(x)}{\partial x}(f(x, h_L(x), 0)-Ax-Bh_L(x)) \\ &\overset{(6b)}{\leq} -c_3|x|^2+\left|\frac{\partial \hat{V}(x)}{\partial x}\right||(\bar{A}-A)x+(\bar{B}-B)h_L(x)+g(x)| \\ &\overset{(6c)}{\leq} -c_3|x|^2+c_4|x|(|(\bar{A}-A)x+(\bar{B}-B)h_L(x)|+|g(x)|)\end{aligned} \tag{9}$$

for all $x \in D_L$. Since the controller $h_L(x)$ is locally Lipschitz, there exists a $K>0$ such that

$$\begin{aligned}\dot{\hat{V}} &\leq -c_3|x|^2+c_4|x|((\|\bar{A}-A\||x|+\|\bar{B}-B\||h_L(x)|)+|g(x)|) \\ &\leq -c_3|x|^2+c_4|x|((\|\bar{A}-A\|+\|\bar{B}-B\|K)|x|+|g(x)|)\end{aligned} \tag{10}$$

for all $x \in B_{\hat{r}}=\{x \in R^n : |x| \leq \hat{r}\}$ where $\hat{r}$ is any $\hat{r} > 0$ such that $B_{\hat{r}} \subset D_L$. If the condition of Eq. 4 is satisfied, there exits a $\delta > 0$ such that

$$\dot{\hat{V}} \leq -c_3|x|^2+c_4\delta|x|^2+c_4|x||g(x)| \tag{11}$$

for all $x \in B_{\hat{r}}$. Since $g(x)$ contains terms of second-order and higher in x and vanishes at the origin, there exists a $\gamma > 0$ such that

$$|g(x)| < \gamma|x|^2 \tag{12}$$

for all $x \in B_{\hat{r}}$. Thus

$$\dot{\hat{V}} \leq -c_3|x|^2+c_4\delta|x|^2+c_4\gamma|x|^3 \tag{13}$$

for all $x \in B_{\hat{r}}$. For any $B_r \subset B_{\hat{r}}$, the time-derivative of $\hat{V}$ can be bounded by the following

$$\dot{\hat{V}} \leq -c_3|x|^2+c_4(\delta+\gamma r)|x|^2 \tag{14}$$

for all $x \in B_r$ where $r < \hat{r}$. If $\delta > 0$ and $r > 0$ are chosen to satisfy $c_3/c_4 > (\delta + \gamma r)$, then there exists a $\hat{c}_3 > 0$ such that

$$\dot{\hat{V}}=\frac{\partial \hat{V}(x)}{\partial x}(f(x, h_L(x), 0)) \leq -\hat{c}_3|x|^2 \tag{15}$$

for all $|x| < r$. Let $\hat{\rho} > 0$ be such that $\hat{\rho} \leq \min\{\hat{V}(x) : |x| < r\}$ which completes the proof. ■

We will make use of the following properties in the "Stability Analysis" subsection. Owing to the locally Lipschitz property assumed for the vector function $f(\cdot, \cdot, \cdot)$ as well as the fact that the Lyapunov function $V(\cdot)$ is a continuously differentiable function, the following inequalities hold

$$|f(x_1, u, w)-f(x_2, u, 0)| \leq L_x|x_1-x_2|+L_w|w|, \tag{16}$$

$$\left|\frac{\partial V(x_1)}{\partial x}f(x_1, u, w)-\frac{\partial V(x_2)}{\partial x}f(x_2, u, 0)\right| \leq L_x'|x_1-x_2|+L_w'|w| \tag{17}$$

for all x_1, $x_2 \in \Omega_{\hat{\rho}}$, $u \in U$ and $|w| \leq \theta$ where L_x, L_w, L_x', and L_w' are positive constants. Additionally, there exists $M > 0$ that bounds the vector field

$$|f(x,u,w)| \leq M \tag{18}$$

for all $x \in \Omega_{\hat{\rho}}, u \in U$ and $|w| \leq \theta$ because $f(\cdot, \cdot, \cdot)$ is a locally Lipschitz vector function of its arguments and Ω_ρ and U are compact sets. For the linear model of Eq. 3, there exist $M_L > 0$ and $L_L > 0$ such that

$$|Ax_1 + Bu| \leq M_L \tag{19}$$

$$\left| \frac{\partial V(x_1)}{\partial x}(Ax_1+Bu) - \frac{\partial V(x_2)}{\partial x}(Ax_2+Bu) \right| \leq L_L|x_1 - x_2| \tag{20}$$

for all $x_1, x_2 \in \Omega_{\hat{\rho}}$ and $u \in U$.

Lyapunov-based EMPC

A specific type of EMPC will be considered in this work. Specifically, we consider LEMPC[3] which utilizes the Lyapunov-based controller $h(x)$ in the design of two constraints. The two constraints allow for provable guarantees on closed-loop stability (the closed-loop state is always bounded in Ω_ρ). Each constraint defines an operating mode of the LEMPC. The formulation of LEMPC is given by the following optimization problem

$$\min_{u \in S(\Delta)} \quad \int_{t_k}^{t_{k+N}} L_e(\tilde{x}(\tau), u(\tau))\ d\tau \tag{21a}$$

$$\text{s.t.} \quad \dot{\tilde{x}}(t) = f(\tilde{x}(t), u(t), 0) \tag{21b}$$

$$\tilde{x}(t_k) = x(t_k) \tag{21c}$$

$$u(t) \in U,\ \forall\ t \in [t_k, t_{k+N}) \tag{21d}$$

$$V(\tilde{x}(t)) \leq \rho_e,\ \forall\ t \in [t_k, t_{k+N}) \quad \text{if } x(t_k) \in \Omega_{\rho_e} \tag{21e}$$

$$\frac{\partial V(x(t_k))}{\partial x} f(x(t_k), u(t_k), 0) \leq \frac{\partial V(x(t_k))}{\partial x} f(x(t_k), h(x(t_k)), 0) \quad \text{if } x(t_k) \notin \Omega_{\rho_e} \tag{21f}$$

where the input trajectory over the prediction horizon $N\Delta$ is the decision variable in the optimization problem. The notation $\tilde{x}(t)$ denotes the predicted behavior of the state trajectory under the input trajectory computed by the LEMPC. The region Ω_{ρ_e} is a subset of the stability region Ω_ρ where time-varying operation is allowed (ρ_e defines a level set of the Lyapunov function and is chosen to make Ω_ρ invariant; see Ref. 3 for details regarding this point).

The objective function of the optimization problem of Eq. 21a is formulated with a stage cost derived from the economics of the system of Eq. 1 (e.g., the operating cost, energy cost, and the negative of the operating profit). The initial value problem embedded in the optimization problem (Eqs. 21b–21c) is used to predict the evolution of the system over the prediction horizon where the initial condition is obtained through a state measurement at the current time step. The input constraint of Eq. 21d bounds the computed input trajectory to be within the admissible input set. Depending on where the current state is in state-space, mode 1, which is defined by the constraint of Eq. 21e, or mode 2, which is defined by the constraint of Eq. 21f, are active. Under mode 1 operation of the LEMPC, the computed input trajectory is allowed to force a potentially transient (time-varying) state trajectory while maintaining the predicted state in a subset of the stability region. The region $\Omega_{\rho_e} \subset \Omega_\rho$ is chosen on the basis of closed-loop stability in the presence of uncertainty, i.e., $w(t) \not\equiv 0$ (as noted above, it is chosen to make Ω_ρ forward invariant). Under mode 2 operation of the LEMPC, the constraint of Eq. 21f forces the control action for the first sampling period in the prediction horizon to decrease the Lyapunov function by at least as much as the decrease forced by the control action computed by the Lyapunov-based controller. This contractive constraint will guarantee that any state starting in $\Omega_\rho \backslash \Omega_{\rho_e}$ will be eventually forced back to Ω_{ρ_e}. For more details and discussion of LEMPC along with a complete closed-loop stability analysis, the interested reader may refer to Ref. 3.

EMPC Using Empirical Models

In this section, we summarize the formulation and implementation of an LEMPC formulated with an empirical model as well as derive sufficient conditions such that the closed-loop nonlinear system under the LEMPC formulated with an empirical model will be stable in a sense to be made precise below.

Formulation with empirical models and implementation

The formulation of the LEMPC with the empirical model is similar to the LEMPC of Eq. 21 except it is formulated with the empirical model of Eq. 3, the stabilizing controller $h_L(x)$, and the Lyapunov function $\hat{V}(x)$. The formulation of the LEMPC using an empirical model is given by

$$\min_{u \in S(\Delta)} \quad \int_{t_k}^{t_{k+N}} L_e(\hat{x}(\tau), u(\tau))\ d\tau \tag{22a}$$

$$\text{s.t.} \quad \dot{\hat{x}}(t) = A\hat{x}(t) + Bu(t) \tag{22b}$$

$$\hat{x}(t_k) = x(t_k) \tag{22c}$$

$$u(t) \in U,\ \forall\ t \in [t_k, t_{k+N}) \tag{22d}$$

$$\hat{V}(\hat{x}(t)) \leq \hat{\rho}_e,\ \forall\ t \in [t_k, t_{k+N}) \quad \text{if } x(t_k) \in \Omega_{\hat{\rho}_e} \tag{22e}$$

$$\frac{\partial \hat{V}(x(t_k))}{\partial x}(Ax(t_k) + Bu(t_k)) \leq \frac{\partial \hat{V}(x(t_k))}{\partial x}(Ax(t_k) + Bh_L(x(t_k))) \quad \text{if } x(t_k) \notin \Omega_{\hat{\rho}_e} \tag{22f}$$

where the notation $\hat{x}(t)$ is used to distinguish that the LEMPC predicts the evolution of the system of Eq. 1 with the empirical model of Eq. 3 and $\Omega_{\hat{\rho}_e} \subset \Omega_{\hat{\rho}}$ is the subset where the LEMPC may dictate a time-varying operating policy (the other constraints are similar to those used in Eq. 21). The optimal solution of the optimization problem of Eq. 22 is denoted as $u^*(t|t_k)$ defined for $t \in [t_k, t_{k+N})$.

The LEMPC of Eq. 22 is implemented in a receding horizon fashion. At a sampling instance, the LEMPC is solved for an input trajectory $u^*(t|t_k)$ for $t \in [t_k, t_{k+N})$, but only applies the control action for the first sampling period of the prediction horizon to the system. The control action to be applied over the first sampling period is denoted as $u^*(t_k|t_k)$. The implementation strategy of the LEMPC is summarized in the following algorithm:

1. Receive a state measurement $x(t_k)$. Go to Step 2.
2. If $x(t_k) \in \Omega_{\hat{\rho}_e}$, go to Step 2.1. Else, go to Step 2.2.
   - 1.1. The mode 1 constraint of Eq. 22e is active and the mode 2 constraint of Eq. 22f is inactive. Go to Step 3.
   - 1.2. The mode 2 constraint of Eq. 22f is active and the mode 1 constraint of Eq. 22e is inactive. Go to Step 3.

3. The optimization problem of Eq. 22 solves for its optimal input trajectory defined for $t \in [t_k,\ t_{k+N})$. Go to Step 4.

4. The first control action of the input trajectory $u^*(t_k|t_k)$ is applied to the system of Eq. 1. Go to Step 5.

5. $k := k+1$ and go to Step 1.

Stability analysis

In this subsection, the stability properties of the LEMPC formulated with the empirical model are analyzed. The following proposition bounds the difference between the actual state trajectory of the system of Eq. 1 in the presence of uncertainty ($w(t) \not\equiv 0$) and the predicted state trajectory from the model of Eq. 3 over a time period from $t=0$ to $t=T$.

Proposition 2. *Consider the solutions, denoted as $x(t)$ and $\hat{x}(t)$, respectively, of the following dynamic equations*

$$\dot{x}(t)=f(x(t),u(t),w(t)),\quad x(0)=x_0, \tag{23}$$

$$\dot{\hat{x}}(t)=A\hat{x}(t)+Bu(t),\quad \hat{x}(0)=x_0, \tag{24}$$

where $u(t) \in U$ and $|w(t)| \le \theta$ for all $t \in [0, T]$ and initial condition $x(0)=\hat{x}(0)=x_0 \in \Omega_{\hat{\rho}}$. If $x(t),\ \hat{x}(t) \in \Omega_{\hat{\rho}}$ for all $t \in [0, T]$, then the difference between $x(T)$ and $\hat{x}(T)$ is bounded by the function $f_w(\cdot)$

$$|x(T)-\hat{x}(T)| \le f_w(T) := \frac{L_w\theta+M_{\rm err}}{L_x}\left(e^{L_xT}-1\right) \tag{25}$$

where $M_{\rm err}$ bounds the difference between right-hand sides of Eqs. 23–24 (with $w(t) \equiv 0$)

$$|f(\hat{x},u,0)-(A\hat{x}+Bu)| \le M_{\rm err} \tag{26}$$

for all $\hat{x} \in \Omega_{\hat{\rho}}$ and $u \in U$.

Proof. Let $e(t)$ be the difference between the state trajectory of Eq. 23 and the state trajectory of Eq. 24 (i.e. $e(t) := x(t)-\hat{x}(t)$) with dynamics $\dot{e}(t)=\dot{x}(t)-\dot{\hat{x}}(t)$ and initial condition $e(0)=0$). The error dynamics can be bounded by

$$\begin{aligned}|\dot{e}(t)| &= |f(x(t),u(t),w(t))-(A\hat{x}(t)+Bu(t))| \\ &\le |f(x(t),u(t),w(t))-f(\hat{x}(t),u(t),0)| \\ &\quad +|f(\hat{x}(t),u(t),0)-(A\hat{x}(t)+Bu(t))|\ .\end{aligned} \tag{27}$$

For a given $\Omega_{\hat{\rho}}$, there exists a $M_{\rm err}>0$ such that

$$|f(\hat{x},u,0)-(A\hat{x}+Bu)| \le M_{err} \tag{28}$$

for all $\hat{x} \in \Omega_{\hat{\rho}}$ and $u \in U$ owing to the Lipschitz property assumed for the vector function $f(\cdot,\cdot,\cdot)$ and the fact that x and u are bounded in compact sets. From Eqs. 27 and 28 and the locally Lipschitz property for $f(\cdot,\cdot,\cdot)$ (Eq. 16), we have the following bound

$$\begin{aligned}|\dot{e}(t)| &\le L_x|x(t)-\hat{x}(t)|+L_w|w(t)|+M_{err} \\ &\le L_x|e(t)|+L_w\theta+M_{err}\end{aligned} \tag{29}$$

for all $t \in [0, T]$ where the last inequality follows from the fact that $|w(t)| \le \theta$. Integrating the bound of Eq. 29 from $t=0$ to $t=T$ gives

$$\int_0^T \frac{|\dot{e}(t)|}{L_x|e(t)|+L_w\theta+M_{err}}\,dt \le T \tag{30}$$

and solving for $|e(T)|$

$$|e(T)|=|x(T)-\hat{x}(T)| \le \frac{L_w\theta+M_{err}}{L_x}\left(e^{L_xT}-1\right) \tag{31}$$

with $x(T),\ \hat{x}(T) \in \Omega_{\hat{\rho}}$.

The next proposition bounds the difference of Lyapunov function values between any two points in $\Omega_{\hat{\rho}}$. The proof may be found in Ref. 42. ■

Proposition 3. (c.f. Ref. 42)

Consider the continuous differentiable Lyapunov function $\hat{V}(\cdot)$ that satisfies the inequalities of Eq. 2. There exists a quadratic function $f_V(\cdot)$ such that

$$\hat{V}(x_1) \le \hat{V}(x_2)+f_V(|x_1-x_2|) \tag{32}$$

for all $x_1,\ x_2 \in \Omega_{\hat{\rho}}$ where

$$f_V(s) := \frac{c_4\sqrt{\hat{\rho}}}{\sqrt{c_1}}s+\beta s^2 \tag{33}$$

and β is a positive constant.

The state feedback controller $h_L(x)$ renders the origin of Eq. 3 asymptotically stable under continuous implementation. In general, the controller $h_L(x)$ implemented in a sample-and-hold fashion may only render the origin of the closed-loop system of Eq. 3 practically stable, that is the closed-loop state of Eq. 3 under the controller $h_L(x)$ implemented in a sample-and-hold is ultimately bounded in a small invariant set containing the origin in its interior. To guarantee a feasible solution to the optimization problem of Eq. 22 under mode 1 operation, the set $\Omega_{\hat{\rho}_e}$ must be larger than the set in which the closed-loop state is ultimately bounded under the controller $h_L(x)$ implemented in a sample-and-hold fashion for a given sampling period $\Delta>0$. The following proposition states sufficient conditions for the minimum size of $\hat{\rho}_e$ for a given Δ needed to guarantee a feasible solution of Eq. 22e under mode 1 operation. To this end, let $\hat{x}(t)$ denote the solution of the sampled-data system resulting from the system of Eq. 3 with the initial condition $\hat{x}(0) \in \Omega_{\hat{\rho}}$ and with the input trajectory obtained from the controller $h_L(x)$ implemented in a sample-and-hold fashion

$$u(t)=h_L(\hat{x}(t_k)) \tag{34}$$

for $t \in [t_k,\ t_{k+1})$, $k=0,\ 1,\ \ldots$with $t_0=0$.

Proposition 4. *Consider the sampled-data system resulting from the system of Eq. 3 under the controller $h_L(x)$ that satisfies the inequalities of Eq. 6 implemented in a sample-and-hold fashion. Let $\Delta>0, \hat{\epsilon}_s>0$, and $\hat{\rho}_e \ge \hat{\rho}_{\min} \ge \hat{\rho}_s>0$ satisfy*

$$-\frac{c_3}{c_2}\hat{\rho}_s+L_LM_L\Delta \le -\hat{\epsilon}_s/\Delta \tag{35}$$

and

$$\hat{\rho}_{\min} := \max\left\{\hat{V}(\hat{x}(t+\Delta))\ :\ \hat{V}(\hat{x}(t)) \le \hat{\rho}_s\right\}\ . \tag{36}$$

If $\hat{x}(0) \in \Omega_{\hat{\rho}_e}$, then $\hat{x}(t) \in \Omega_{\hat{\rho}_e}$ for all $t \ge 0$ and

$$\hat{V}(\hat{x}(t_{k+1}))-\hat{V}(\hat{x}(t_k)) \le -\hat{\epsilon}_s \tag{37}$$

for $\hat{x}(t_k) \in \Omega_{\hat{\rho}_e}\backslash\Omega_{\hat{\rho}_s}$ and $\hat{x}(t)$ is ultimately bounded in $\Omega_{\hat{\rho}_{\min}}$.

Proof. Consider the sampled-data system resulting from the system of Eq. 3 under the controller $h_L(x)$ applied in a sample-and-hold fashion. At each sampling period t_k, the input trajectory obtained from the controller $h_L(x)$ applied in a sample-and-hold fashion has the following property

$$\frac{\partial \hat{V}(\hat{x}(t_k))}{\partial x}(A\hat{x}(t_k)+Bh_L(\hat{x}(t_k))) \le -c_3|\hat{x}(t_k)|^2 \quad (38)$$

from Eq. 6b. For simplicity of notation, let $\hat{u}(t_k) := h_L(\hat{x}(t_k))$. Consider the time-derivative of the Lyapunov function for the empirical model for $\tau \in [t_k, t_{k+1})$

$$\begin{aligned}\frac{\partial \hat{V}(\hat{x}(\tau))}{\partial x}(A\hat{x}(\tau)+B\hat{u}(t_k)) &= \frac{\partial \hat{V}(\hat{x}(\tau))}{\partial x}(A\hat{x}(\tau)+B\hat{u}(t_k)) \\ &\quad - \frac{\partial \hat{V}(\hat{x}(t_k))}{\partial x}(A\hat{x}(t_k)+B\hat{u}(t_k)) \\ &\quad + \frac{\partial \hat{V}(\hat{x}(t_k))}{\partial x}(A\hat{x}(t_k)+B\hat{u}(t_k)) \\ &\le L_L|\hat{x}(\tau)-\hat{x}(t_k)|-c_3|\hat{x}(t_k)|^2\end{aligned} \quad (39)$$

where the last inequality follows from Eqs. 38 and 20. Owing to continuity of solutions in a compact set and the bound of Eq. 19, the following bound holds

$$|\hat{x}(\tau)-\hat{x}(t_k)| \le M_L\Delta \quad (40)$$

for $\tau \in [t_k, t_{k+1}]$. From Eq. 39 and Eq. 40, the time derivative of the Lyapunov function is bounded by

$$\frac{\partial \hat{V}(\hat{x}(\tau))}{\partial x}(A\hat{x}(\tau)+B\hat{u}(t_k)) \le -c_3|\hat{x}(t_k)|^2+L_LM_L\Delta \quad (41)$$

for $\tau \in [t_k, t_{k+1})$.

If $\Delta > 0$ is sufficiently small such that there exist $\hat{\rho}_s > 0, \hat{\rho}_{\min} > 0$, and $\hat{\epsilon}_s > 0$ with $\hat{\rho}_e \ge \hat{\rho}_{\min}$ defined according to Eqs. 35 and 36, the state $\hat{x}(t)$ remains bounded in $\Omega_{\hat{\rho}_e}$ for $t \ge 0$ when $\hat{x}(0) \in \Omega_{\hat{\rho}_e}$. To show this, we need to consider two cases: $\hat{x}(t_k) \in \Omega_{\hat{\rho}_e} \backslash \Omega_{\hat{\rho}_s}$ and $\hat{x}(t_k) \in \Omega_{\hat{\rho}_s}$. When $\hat{x}(t_k) \in \Omega_{\hat{\rho}_e} \backslash \Omega_{\hat{\rho}_s}$ and $\hat{x}(\tau) \in \Omega_{\hat{\rho}_e}$ for $\tau \in [t_k, t_{k+1})$, the following bound on the time derivative of the Lyapunov function can be written from the inequalities of Eqs. 41 and 6a

$$\frac{\partial \hat{V}(\hat{x}(\tau)))}{\partial x}(A\hat{x}(\tau)+B\hat{u}(t_k)) \le -\frac{c_3}{c_2}\hat{\rho}_s+L_LM_L\Delta \quad (42)$$

for $\tau \in [t_k, t_{k+1})$. If the condition of Eq. 35 holds, there exists a $\hat{\epsilon}_s > 0$ such that

$$\frac{\partial \hat{V}(\hat{x}(\tau)))}{\partial x}(A\hat{x}(\tau)+B\hat{u}(t_k)) \le -\hat{\epsilon}_s/\Delta \quad (43)$$

for $\tau \in [t_k, t_{k+1})$. Integrating the bound for $\tau \in [t_k, t_{k+1}]$, we have

$$\begin{aligned}\hat{V}(\hat{x}(t_{k+1})) &\le \hat{V}(\hat{x}(t_k))-\hat{\epsilon}_s, \\ \hat{V}(\hat{x}(\tau)) &\le \hat{V}(\hat{x}(t_k)), \quad \forall\ \tau \in [t_k, t_{k+1}]\end{aligned} \quad (44)$$

for all $\hat{x}(t_k) \in \Omega_{\hat{\rho}_e} \backslash \Omega_{\hat{\rho}_s}$ which shows the result of Eq. 37 and $x(t) \in \Omega_{\hat{\rho}_e}$ for all $t \in [t_k, t_{k+1}]$.

For any $\hat{x}(t_k) \in \Omega_{\hat{\rho}_e} \backslash \Omega_{\hat{\rho}_s}$, we showed that the Lyapunov function under the controller $h_L(x)$ applied in a sample-and-hold fashion will decrease at the next sampling period. When $\hat{x}(t_k) \in \Omega_{\hat{\rho}_s}$ and there exists a $\hat{\rho}_{\min} \le \hat{\rho}_e$ defined according to Eq. 36, the state is ultimately bounded in $\Omega_{\hat{\rho}_{\min}}$ under the Lyapunov-based controller applied in a sample-and-hold fashion owing to the definition of $\hat{\rho}_{\min}$. Thus, $\Omega_{\hat{\rho}_e}$ is forward invariant for the sampled-data system resulting from the system of Eq. 3 under the Lyapunov-based controller implemented in a sample-and-hold fashion (i.e., there exists a sample-and-hold trajectory with sampling period Δ that maintains $\hat{x}(t)$ in $\Omega_{\hat{\rho}_e}$). ■

Remark 1. *It is possible to show stronger notions of stability for the closed-loop system of Eq. 3 under the controller $h_L(x)$ applied in a sampled-and-hold fashion. For example, when the controller $h_L(x)$ is applied in a sample-and-hold fashion with a sufficiently small sampling period to the system of Eq. 3, the origin will be exponentially stable (see, for example, Ref. 43 for results in this direction). However, these stronger notions of stability are not needed in the context of the closed-loop stability results for the system of Eq. 1 under the LEMPC of Eq. 22.*

The purpose of $\Omega_{\hat{\rho}_e}$ is to make $\Omega_{\hat{\rho}}$ invariant for the closed-loop system of Eq. 1 under the LEMPC of Eq. 22. The condition on $\hat{\rho}_e$ along with other sufficient conditions such that the closed-loop state trajectory of Eq. 1 under the LEMPC of Eq. 22 is always maintained in $\Omega_{\hat{\rho}}$ are given in the following theorem.

Theorem 1. *Consider the closed-loop system of Eq. 1 under the LEMPC of Eq. 22 based on the controller $h_L(x)$ that satisfies the inequalities of Eq. 6. Let $\epsilon_w > 0$, $\Delta > 0$, $N \ge 1$, and $\hat{\rho} > \hat{\rho}_e > 0$ satisfy*

$$-\frac{\hat{c}_3}{c_2}\hat{\rho}_e+L_x'M\Delta+L_w'\theta \le -\epsilon_w/\Delta\ , \quad (45)$$

$$\hat{\rho}_e \le \hat{\rho}-f_V(f_w(\Delta))\ . \quad (46)$$

If $x(0) \in \Omega_{\hat{\rho}}$ and the conditions of Proposition 1 and Proposition 4 are satisfied, then the state trajectory x(t) of the closed-loop system is always bounded in $\Omega_{\hat{\rho}}$ for $t \ge 0$.

Proof. The proof is divided into two parts. In *Part 1*, feasibility of the LEMPC optimization problem is proved when the state is maintained in $\Omega_{\hat{\rho}}$. Subsequently, the closed-loop state under the LEMPC of Eq. 22 is shown to be always bounded in $\Omega_{\hat{\rho}}$ in *Part 2*.

Part 1. If mode 1 operation of the LEMPC of Eq. 22 is active ($x(t_k) \in \Omega_{\hat{\rho}_e}$) and the conditions of Proposition 4 are satisfied (i.e., there exist positive constants $\hat{\rho}_s, \hat{\rho}_{\min}$, and $\hat{\epsilon}_s$ that satisfy Eqs. 35–36), the LEMPC (under mode 1 operation) is feasible because the sample-and-hold trajectory obtained from the controller $h_L(x)$ is a feasible solution to the LEMPC optimization problem which follows from Proposition 4. When the current state $x(t_k) \in \Omega_{\hat{\rho}} \backslash \Omega_{\hat{\rho}_e}$ and the LEMPC of Eq. 22 operates in mode 2 operation, the optimization problem is feasible because the input trajectory $u(t) = h_L(x(t_k))$ for $t \in [t_k, t_{k+1})$ and any piecewise constant trajectory $u(t) \in U$ for $t \in [t_{k+1}, t_{k+N})$ will satisfy the input constraint of Eq. 22d and the mode 2 constraint of Eq. 22f. Thus, the LEMPC is recursively feasible if the closed-loop state is maintained in $\Omega_{\hat{\rho}}$.

Part 2. Consider the closed-loop state trajectory under the LEMPC of Eq. 22. If $x(t_k) \in \Omega_{\hat{\rho}} \backslash \Omega_{\hat{\rho}_e}$, the LEMPC operates in mode 2 (the constraint of Eq. 22f is active) and the computed input satisfies

$$\frac{\partial \hat{V}(x(t_k))}{\partial x}(Ax(t_k)+Bu(t_k)) \le \frac{\partial \hat{V}(x(t_k))}{\partial x}(Ax(t_k)+Bh_L(x(t_k))) \quad (47)$$

for all $x(t_k) \in \Omega_{\hat{\rho}} \backslash \Omega_{\hat{\rho}_e}$. From Proposition 1 (Eq. 15), for δ and $\hat{\rho}$ sufficiently small, there exists a $\hat{c}_3 > 0$ such that

$$\frac{\partial \hat{V}(x(t_k))}{\partial x}f(x(t_k), h_L(x(t_k)), 0) \le -\hat{c}_3|x(t_k)|^2 \quad (48)$$

The time derivative of the Lyapunov function (of the closed-loop nonlinear system) over the sampling period is

$$\dot{\hat{V}}(x(\tau)) = \frac{\partial \hat{V}(x(\tau))}{\partial x} f(x(\tau), h_L(x(t_k)), w(\tau)) - \frac{\partial \hat{V}(x(t_k))}{\partial x} f(x(t_k), h_L(x(t_k)), 0) + \frac{\partial \hat{V}(x(t_k))}{\partial x} f(x(t_k), h_L(x(t_k)), 0)$$

$$\overset{(17),(48)}{\leq} L_x' |x(\tau) - x(t_k)| + L_w' |w(\tau)| - \hat{c}_3 |x(t_k)|^2 \leq -\frac{\hat{c}_3}{c_2} \hat{\rho}_e + L_x' |x(\tau) - x(t_k)| + L_w' |w(\tau)| \quad (49)$$

for $\tau \in [t_k, t_{k+1})$ where the last inequality follows from the fact that $x(t_k) \in \Omega_{\hat{\rho}} \backslash \Omega_{\hat{\rho}_e}$ and the bound of Eq. 6a. From Eq. 18 and the continuity of solutions, the difference between $x(\tau)$ and $x(t_k)$ is bounded

$$|x(\tau) - x(t_k)| \leq M\Delta \quad (50)$$

for all $\tau \in [t_k, t_{k+1})$. From Eqs. 49 and 50 and the fact that the disturbance vector is bounded ($|w(\tau)| \leq \theta$), we have

$$\frac{\partial \hat{V}(x(\tau))}{\partial x} f(x(\tau), u(t_k), 0) \leq -\frac{\hat{c}_3}{c_2} \hat{\rho}_e + L_x' M\Delta + L_w' \theta \quad (51)$$

for all $\tau \in [t_k, t_{k+1})$. If the condition of Eq. 45 is satisfied, then the following can be derived

$$\begin{aligned} \hat{V}(x(t_{k+1})) &\leq \hat{V}(x(t_k)) - \epsilon_w, \\ \hat{V}(x(\tau)) &\leq \hat{V}(x(t_k)), \quad \forall\ \tau \in [t_k, t_{k+1}] \end{aligned} \quad (52)$$

for all $x(t_k) \in \Omega_{\hat{\rho}} \backslash \Omega_{\hat{\rho}_e}$ by employing the same steps used to derive the equations of Eq. 44. Thus, when the LEMPC operates in mode 2, the Lyapunov function value will decrease at the next sampling period and converge to the set $\Omega_{\hat{\rho}_e}$ in a finite number of sampling periods.

If $x(t_k) \in \Omega_{\hat{\rho}_e}$, the LEMPC will operate in mode 1. The predicted state at the next sampling period must be in $\Omega_{\hat{\rho}_e}$ ($\hat{x}(t_{k+1}) \in \Omega_{\hat{\rho}_e}$) which is enforced by the constraint of Eq. 22e. By Propositions 2 and 3, we have

$$\begin{aligned} \hat{V}(x(t_{k+1})) &\leq \hat{V}(\hat{x}(t_{k+1})) + f_V(|x(t_{k+1}) - \hat{x}(t_{k+1})|) \\ &\leq \hat{\rho}_e + f_V(f_w(\Delta)) \end{aligned} \quad (53)$$

If the condition of Eq. 46 is satisfied, $x(t_{k+1}) \in \Omega_{\hat{\rho}}$. Thus, under mode 1 and mode 2 operation of the LEMPC, the closed-loop state is maintained in $\Omega_{\hat{\rho}}$ which completes the proof. ■

Remark 2. *Since the empirical model of Eq. 3 can only accurately predict the behavior of the system of Eq. 1 within a limited region in state space, it may be difficult to find an empirical model that can adequately capture the dynamics of the system of Eq. 1 for use in EMPC. The accuracy of the model used in EMPC is critical because it affects both the closed-loop performance and stability. A strategy to improve the accuracy of the model of Eq. 3 is to use multiple empirical models for different regions of state space to better capture the nonlinear dynamics of Eq. 1 and as a result of the increased accuracy, use a larger $\Omega_{\hat{\rho}}$ than what is possible (from a closed-loop stability perspective) with a single empirical model.*

Remark 3. *The general heuristic is that the closed-loop economic performance improves with increasing prediction horizon when applying nonlinear EMPC (i.e., EMPC formulated with a nonlinear model). However, when using EMPC with an empirical model, the predicted behavior of the system obtained from the empirical model over a long horizon may be significantly different than the actual nonlinear behavior. Thus, increasing the prediction horizon of EMPC with an empirical model may not increase the performance. In other words, the accuracy of the prediction by the empirical model may affect the closed-loop performance and it may be better from a closed-loop performance standpoint to restrict operation to a smaller region state-space where the empirical model can provide a sufficient degree of accuracy.*

Remark 4. *As a by-product of using an empirical model in LEMPC, the computational efficiency of LEMPC is improved in general compared to using a nonlinear model in LEMPC since a linear model is used in the optimization problem instead of a nonlinear model and the empirical model of Eq. 3 can be converted to an exact discrete-time model with zeroth-order sample-and-hold inputs (i.e., no need to embed a numerical ordinary differential equation solver to solve the dynamic optimization problem of the LEMPC). Thus, one may consider using an empirical model even when a nonlinear model is available owing to the improved computational efficiency. This point will be demonstrated in the "Application to a Chemical Process Example" section.*

Remark 5. *It is important to emphasize that at each sampling time the LEMPC of Eq. 22 is re-initialized with a state measurement. This incorporation of feedback allows for the LEMPC of Eq. 22 to maintain robustness to disturbances.*

Table 1. Parameter Values of the CSTR

$T_0 = 300$	K	$F = 5.0$	m^3/h
$V = 1.0$	m^3	$E = 5.0 \times 10^4$	kJ/kmol
$k_0 = 8.46 \times 10^6$	m^3/h/kmol	$\Delta H = -1.15 \times 10^4$	kJ/kmol
$C_p = 0.231$	kJ/kg/K	$R = 8.314$	kJ/kmol/K
$\rho_L = 1000$	kg/m^3		

Application to a Chemical Process Example

Consider a nonisothermal, well-mixed continuous stirred tank reactor (CSTR) where an irreversible, second-order, exothermic reaction occurs. The reaction converts the reactant A to the product B and is of the form $A \rightarrow B$. The feedstock of the reactor contains A in an inert solvent and the inlet concentration of A is C_{A0}, inlet temperature is T_0, and feed volumetric flow rate is F. A jacket is used to heat/cool the reactor at heat rate Q. The liquid density ρ_L, heat capacity C_p, and liquid hold-up V are assumed to be constant. The dynamic model equations describing the evolution of the CSTR, obtained by applying standard modeling assumptions and mass and energy balances to the reactor, are presented below

$$\frac{dC_A}{dt} = \frac{F}{V}(C_{A0} - C_A) - k_0 e^{-E/RT} C_A^2 \quad (54a)$$

$$\frac{dT}{dt} = \frac{F}{V}(T_0 - T) - \frac{\Delta H k_0}{\rho_L C_p} e^{-E/RT} C_A^2 + \frac{Q}{\rho_L C_p V} \quad (54b)$$

where C_A and T are the reactant A concentration in the reactor and reactor temperature, respectively. The notation k_0, E, ΔH denotes the pre-exponential factor, activation energy of the reaction, and the enthalpy of the reaction, respectively. The values of the process parameters are given in Table 1. In the simulations below, the explicit Euler method with an

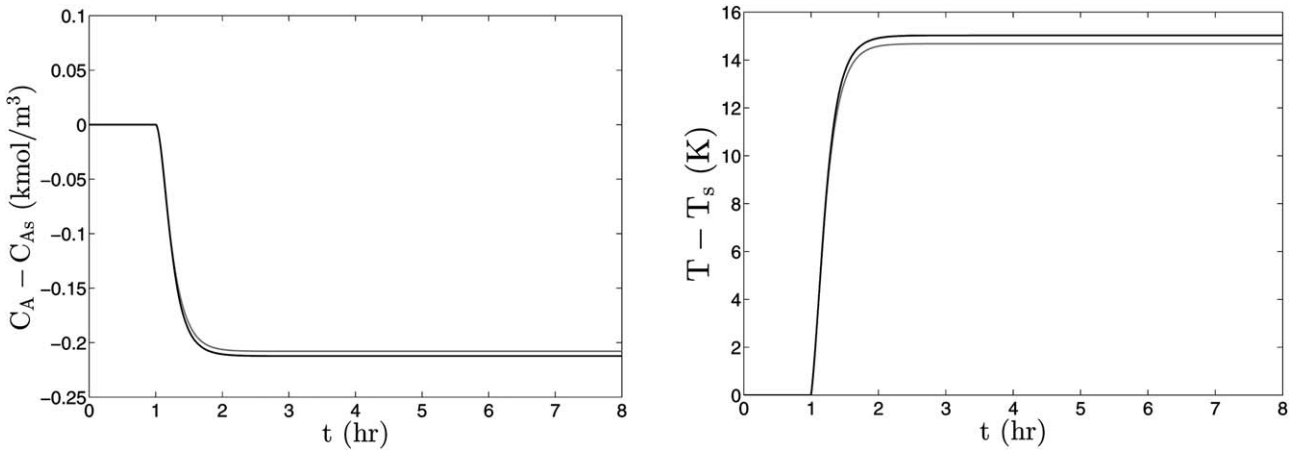

Figure 1. Response of the CSTR of Eq. 54 (black line) to a step input compared to the response predicted by the identified linear model of Eq. 57 (gray line).

The step is in the heat rate input (u_2) starting at 1 h with a magnitude of 5000 kJ/h.

integration time step of $h_c = 10^{-4}$ h was used to integrate the dynamic model of Eq. 54.

The inlet concentration C_{A0} and the heat supply/removal rate Q are the two manipulated inputs of the CSTR. The manipulated inputs are bounded as follows: $0.5 \leq C_{A0} \leq 7.5$ kmol/m^3 and $-5.0 \times 10^5 \leq Q \leq 5.0 \times 10^5$ kJ/h. The control objective is to maximize the time-averaged production rate of the product B by operating the CSTR in a compact state-space set around the operating steady-state of the CSTR. To this end, the operating steady-state vector of the CSTR is $[C_{As}\ T_s] = [1.2$ kmol/m^3 438.0 K$]$ and the corresponding steady-state input vector is $[C_{A0s}\ Q_s] = [4.0$ kmol/m^3 0.0 kJ/h$]$. The steady-state is open-loop asymptotically stable. The state and input vector of the CSTR are defined using deviation variables: $x^T = [C_A - C_{As}\ T - T_s]$ is the state vector and $u^T = [C_{A0} - C_{A0s}\ Q - Q_s]$ is the manipulated input vector. The production rate of B is given by the reaction rate $k_0 e^{-E/RT} C_A^2$. In the theoretical developments, the LEMPC of Eq. 21 is written to minimize the objective function. Thus, to maximize the production rate of B in the example, the economic cost function is the negative of the production rate of B and is given by

$$L_e(x,u) = -\frac{1}{(t_{k+N} - t_k)} \int_{t_k}^{t_{k+N}} k_0 e^{-E/RT(\tau)} C_A^2(\tau)\ d\tau\,. \qquad (55)$$

In addition, we consider that there is a limitation on the amount of reactant material that may be fed to the CSTR during a given period of operation t_p. Therefore, the control input trajectory of u_1 should satisfy the following material constraint

$$\frac{1}{t_p} \int_0^{t_p} u_1(\tau)\ d\tau = 0.0\,\text{kmol/m}^3 \qquad (56)$$

where $t_p = 1.0$ h is the operating period length to enforce the material constraint.

Model identification and validation

We assume that for the CSTR, the nonlinear model of Eq. 54 is not available and a model needs to be identified and validated. The model will be fit using standard input/output data-based techniques (recall that state feedback is assumed, so the output is the state) to identify a linear time invariant state-space model. A series of step inputs were used to generate the input/output data. An iterative process was employed to identify and validate the model. First, a step input sequence was generated and applied to the CSTR. From the input/output data, the ordinary MOESP[24] algorithm was used to regress a linear model of the CSTR of Eq. 54. Step, impulse, and sinusoidal input responses were used to validate the model. Additionally, an LEMPC scheme of the form described below in the subsequent subsection was designed using the empirical model. The LEMPC with the identified model was applied to the CSTR of Eq. 54. Extensive closed-loop simulations with the LEMPC were performed to confirm closed-loop stability and acceptable closed-loop performance under the resulting LEMPC. From these validation experiments (input response tests and the closed-loop simulations), a model was identified and validated.

The identified matrices for the linear model of the CSTR (in continuous-time) are

$$A = \begin{bmatrix} -34.5 & -0.473 \\ 1430 & 18.1 \end{bmatrix},\ B = \begin{bmatrix} 5.24 & -8.09\times10^{-6} \\ -11.6 & 4.57\times10^{-3} \end{bmatrix} \qquad (57)$$

where the state-space coordinates correspond to the coordinates used in the nonlinear model of Eq. 54. The step, impulse, and sinusoidal input responses are shown in Figures 1–3. From Figures 1–3, the predicted response of the CSTR using the identified linear model is close to the response of the actual nonlinear system of Eq. 54.

Application of LEMPC based on an empirical model

Before an LEMPC may be designed, a Lyapunov-based controller is designed, a Lyapunov function under the Lyapunov-based controller is constructed, and the stability region of the CSTR under the Lyapunov-based controller is estimated. Since we assume that only the empirical model is available, we work with the empirical model to design the Lyapunov-based controller. The Lyapunov-based controller consists of two elements for each input: $h_L^T(x) = [h_1(x)\ h_2(x)]$, and the inlet concentration input is fixed to 0.0 kmol/m^3 to satisfy the material constraint of Eq. 56 ($h_1(x) = 0$). Defining the vector and matrix functions f: $R^n \rightarrow R^n$ and g: $R^n \rightarrow R^n \times R^m$ as follows

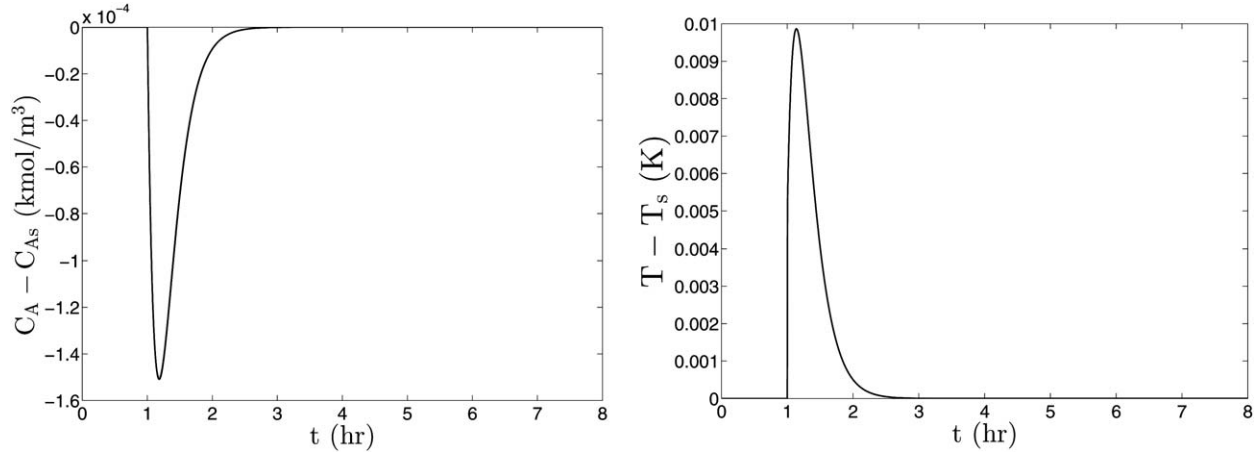

Figure 2. Response of the CSTR of Eq. 54 (black line) to an impulse input compared to the response predicted by the identified linear model of Eq. 57 (gray line) which are nearly overlapping.

To numerically simulate the impulse, a rectangular pulse of magnitude 1500 kJ/h in the heat rate input was applied for 36 s.

$$\dot{x} = \underbrace{Ax}_{=:f(x)} + \underbrace{B}_{=:g(x)} u \ , \tag{58}$$

the following control law is used for the heat rate input in the Lyapunov-based controller[44]

$$h_2(x) = \begin{cases} -\dfrac{L_f\hat{V} + \sqrt{L_f\hat{V}^2 + L_{g_2}\hat{V}^4}}{L_{g_2}\hat{V}}, & \text{if } L_{g_2}\hat{V} \neq 0 \\ 0, & \text{if } L_{g_2}\hat{V} = 0 \end{cases} \tag{59}$$

where $L_f\hat{V}$ is the Lie derivative of the Lyapunov function $\hat{V}(x)$ with respect to the vector field $f(x)$ and the notation $g_2(x)$ denotes the second column of B. A quadratic Lyapunov function of the form: $\hat{V}(x) = x^T P x$ where P is the following positive definite matrix

$$P = \begin{bmatrix} 1060 & 22 \\ 22 & 0.52 \end{bmatrix} \tag{60}$$

was used. After extensive closed-loop simulations under the Lyapunov-based controller and under the LEMPC designed on the basis of the Lyapunov-based controller $h(x)$ and with the model of Eq. 57, the level sets $\Omega_{\hat{\rho}}$ and $\Omega_{\hat{\rho}_e}$, which will be used in the LEMPC, were estimated to be $\hat{\rho} = 64.3$ (i.e., $\Omega_{\hat{\rho}} = \{x \in R^n : \hat{V}(x) \leq \hat{\rho}\}$), and $\hat{\rho}_e = 55.0$, respectively. The sampling period and prediction horizon of the LEMPC are $\Delta = 0.01$ h and $N = 10$, respectively.

An LEMPC scheme of the form of Eq. 22 was designed utilizing the model of Eq. 57 for the CSTR with the cost function of Eq. 55 and the material constraint of Eq. 56. The material constraint of Eq. 56 is enforced over each 1.0 h operating period using the strategy described in Ref. 5. To solve the LEMPC optimization problem at each sampling period, the interior point solver Ipopt was employed.[45] To make the simulations more realistic, the solver was forced to terminate solving and return a solution by the end of the sampling period although instantaneous availability of the control action at the current sampling time is assumed in the closed-loop simulations. For the remainder, nonlinear LEMPC will refer to an LEMPC scheme formulated with the nonlinear dynamic model of Eq. 54, while linear LEMPC will refer to an LEMPC scheme formulated with the linear model of Eq. 57. In the following simulations, both nonlinear LEMPC and linear LEMPC were considered as a baseline comparison. While this comparison may be done

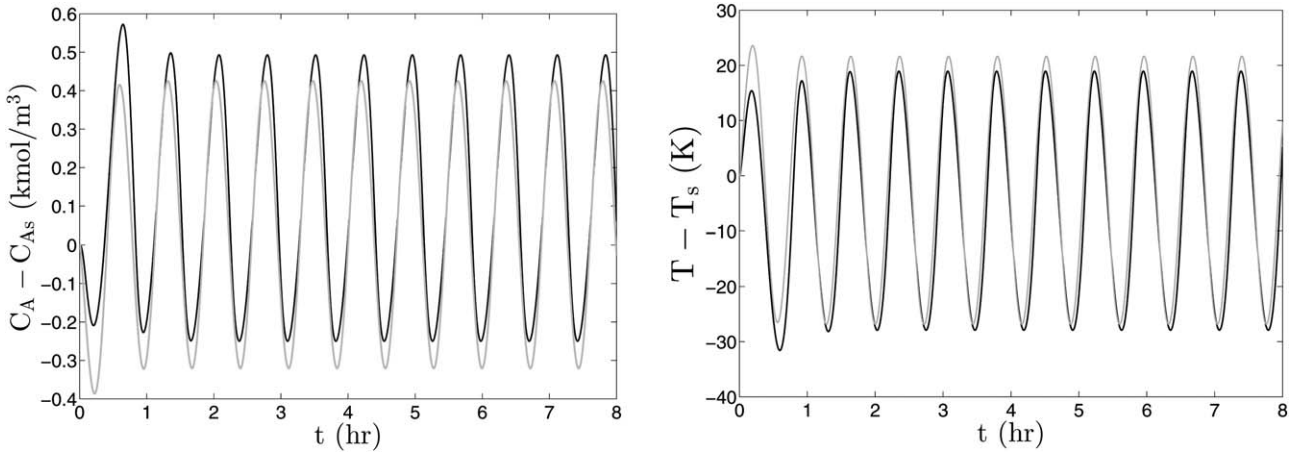

Figure 3. Response of the CSTR of Eq. 54 (black line) to a sinusoidal input response compared to the response predicted by the identified linear model of Eq. 57 (gray line).

The amplitude of the heat rate input sinusoid is 30,000 kJ/h with a frequency of 8.72 rad/h.

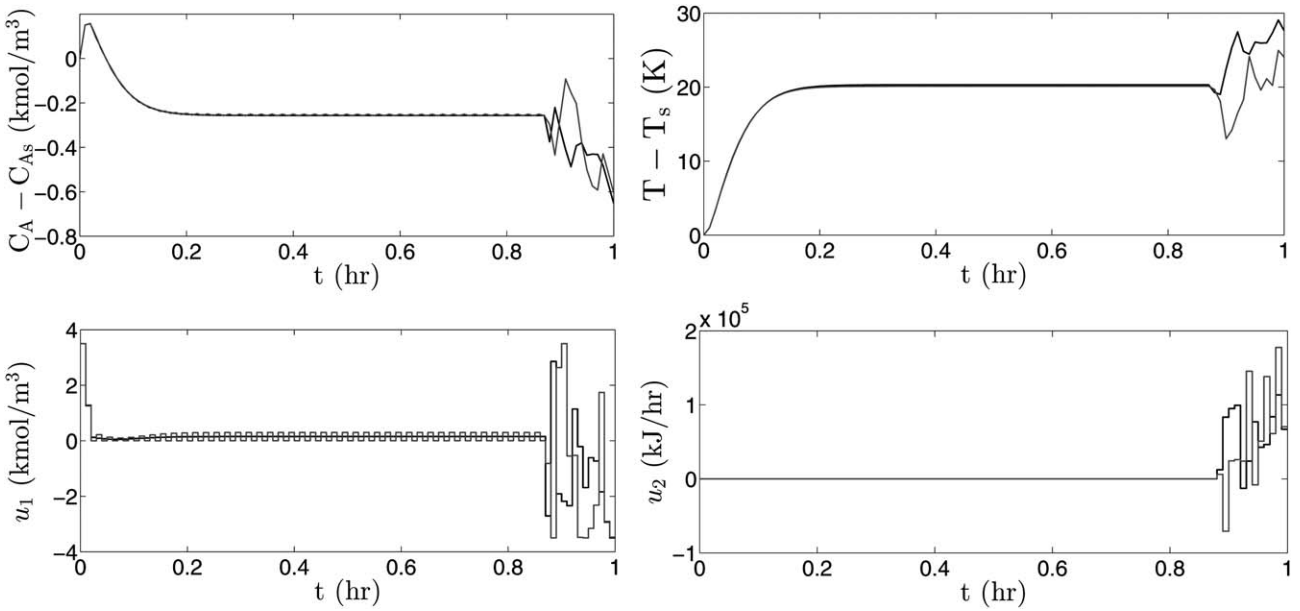

Figure 4. The state and input profiles of the closed-loop CSTR under the nonlinear LEMPC (black line) and under the linear LEMPC (gray line) for the initial condition: $C_A(0) = 1.2$ kmol/m^3 and $T(0) = 438$ K.

through simulations, a nonlinear model may not be available and thus, this type of comparison may not be able to be completed in practice. For the nonlinear LEMPC simulations, only mode 1 operation of the controller was considered since the nonlinear LEMPC is able to maintain operation within $\Omega_{\hat{\rho}_e}$ under nominal operation. To solve the initial value problem embedded in the optimization problem, the explicit Euler method was used for the nonlinear LEMPC, and the discrete-time version of the model of Eq. 57 with a zero-order hold of the inputs with sampling period $\Delta = 0.01$ h was used in the linear LEMPC.

Linear LEMPC compared with nonlinear LEMPC

Both the nonlinear and linear LEMPC were applied to the CSTR of Eq. 54, and a closed-loop simulation over one operating period (1 h) was completed for each case. The CSTR was initialized at the steady-state: $C_A(0) = 1.2$ kmol/m^3 and $T(0) = 438.0$ K. The closed-loop trajectories for the CSTR under both LEMPC schemes are shown in Figure 4. The trajectories of the two cases demonstrate a similar behavior with three distinct phases. In the first phase, the LEMPC forces the CSTR from the initial condition to a greater temperature to increase the production rate of B. In the second phase, the trajectories settle on an equilibrium point located at the boundary of $\Omega_{\hat{\rho}_e}$ from approximately 0.2–0.8 h. This steady state has a greater temperature than the operating steady-state ($C_{As} = 1.2$ kmol/m^3 and $T_s = 438.0$ K). Finally, to achieve additional economic performance benefit at the end of the operating period and to satisfy the material constraint, the LEMPC forces the state away from the steady state to a greater temperature. Perhaps, the two most noticeable differences in the closed-loop trajectories of Figure 4, are the oscillations or chattering observed in the u_1 trajectory computed by the linear LEMPC and the differences in the trajectories at the end of the operating period. The oscillations are caused by the linear LEMPC switching between mode 1 and mode 2 operations of the controller. Given the fact that the linear LEMPC uses an inexact model, it cannot compute a control action that exactly maintains the actual state at the boundary of $\Omega_{\hat{\rho}_e}$. A state starting in $\Omega_{\hat{\rho}_e}$ may leave $\Omega_{\hat{\rho}_e}$ under the linear LEMPC. However, it will still be contained in $\Omega_{\hat{\rho}}$ at the next sampling period by design of $\Omega_{\hat{\rho}_e}$. Once the state is in $\Omega_{\hat{\rho}} \backslash \Omega_{\hat{\rho}_e}$, the linear LEMPC switches to mode 2 operation to force the state back into $\Omega_{\hat{\rho}_e}$. The linear LEMPC operates in mode 1 operation after the state converges back to $\Omega_{\hat{\rho}_e}$. On the other hand, the nonlinear LEMPC is able to maintain the LEMPC at the boundary of $\Omega_{\hat{\rho}_e}$ since we are considering nominal operation (i.e., the LEMPC uses an exact model of the CSTR to compute its control action). Thus, the nonlinear LEMPC is able to maintain operation in $\Omega_{\hat{\rho}_e}$, so the controller always operates in mode 1 operation. To better observe the differences between the closed-loop state trajectories, the closed-loop trajectories for each of the two previous simulations are shown in state space (Figure 5). From Figure 5, noticeable differences between the evolution of the two cases at the end of the operating period is observed. In the region of operation at the end of the operating period, the linear model is less accurate and hence, the linear LEMPC computes a different input trajectory than the nonlinear LEMPC.

The fact that a similar trend was observed between the closed-loop CSTR under the nonlinear LEMPC, which uses the exact dynamic model, and the linear LEMPC, which uses a linear model identified through input/output data, is a positive result for EMPC using an empirical model. It indicates that one may be able to use standard identification techniques to identify an empirical model for use within the context of EMPC when a nonlinear model is not available. However, it is also important to investigate the advantages and disadvantages and possible trade-offs of using nonlinear LEMPC (when a nonlinear model is available) and using linear LEMPC. To quantify the closed-loop performance of each case, we define the average economic cost index as

$$J_e = \frac{1}{t_f} \int_0^{t_f} k_0 e^{-E/RT(t)} C_A^2(t)\ dt \tag{61}$$

where t_f is the length of simulated closed-loop operation. For simplicity of presentation, the units on the average economic

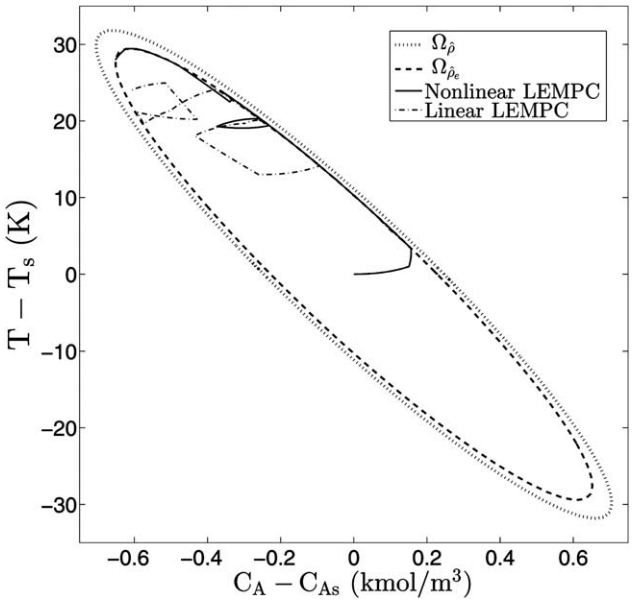

Figure 5. The state trajectories of the CSTR under: nonlinear LEMPC (solid line) and linear LEMPC (dashed-dotted line).

cost index, which are kmol/m^3, are omitted. For the linear LEMPC, the economic cost index is 15.70, while the economic cost index of the closed-loop CSTR under the nonlinear LEMPC is 15.77. For an 1 h operating period, applying nonlinear LEMPC achieves less than a 0.5% improvement of the economic cost index compared to the economic cost under the linear LEMPC.

The computation time required to solve the LEMPC optimization problem at each sampling period was also considered for the nonlinear and linear LEMPCs. Figure 6 shows the computation time required to solve the nonlinear and linear LEMPC at each sampling period, respectively. The higher computation time observed at the end of the operating period in each of the cases is associated with the fact that the constraints are active (the constraint to maintain operation in $\Omega_{\hat{\rho}_e}$ and the average input constraint). From Figure 6, the optimization solver terminated early four times for the nonlinear LEMPC (recall that the solver was constrained to return a solution after 36 s of computation time). For this case, the total amount of computation time required to solve the LEMPC optimization problem over all the sampling periods was 193 s. For the linear LEMPC, early termination of the optimization solver was never experienced and for most of the sampling periods, the solver converged in less than 0.1 s (Figure 6). The total computation time required to solve the linear LEMPC at each sampling period in the simulation was 22 s; the total time required to solve the nonlinear LEMPC at each sampling period is 777% greater than the computation time required to solve the linear LEMPC.

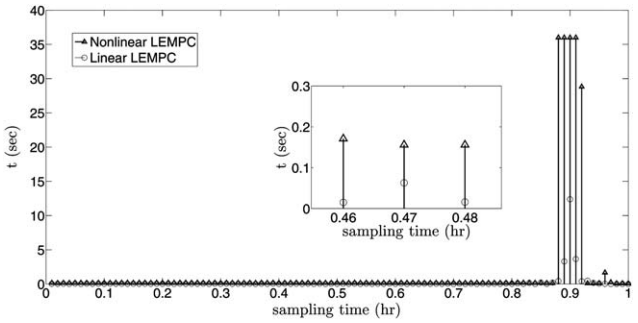

Figure 6. The computation time in seconds required to solve the nonlinear LEMPC (triangle markers) and the linear LEMPC (circle markers) optimization problem at each sampling period.

To demonstrate the application of the linear LEMPC to the CSTR of Eq. 54 over many operating periods, a closed-loop simulation of 10 h was completed. The closed-loop trajectories are shown in Figures 7–10. The closed-loop economic performance as measured by the average economic cost of Eq. 61 was 15.29. Maintaining the CSTR at the initial condition, which is the steady-state, has an average economic cost of 13.88 (the linear LEMPC dictates an operating policy that is 10% better than operating the CSTR at the operating steady-state). As a comparison, a simulation of the CSTR under the nonlinear LEMPC over 10 h was performed. The closed-loop trajectories of the CSTR under the nonlinear LEMPC were similar to those under the linear LEMPC except that: the closed-loop u_1 trajectory computed by the nonlinear LEMPC did not have chattering like the closed-loop u_1 trajectory computed by the linear LEMPC (Figure 8) for reasons stated above and the other differences in the closed-loop trajectories noted above for the 1 h simulations were also observed. The average economic cost of the closed-loop CSTR under the nonlinear LEMPC was 15.40. The closed-loop performance under the nonlinear LEMPC is 0.7% better than that achieved under linear LEMPC. However, the average total computation time required to solve the nonlinear LEMPC optimization problem over each operating period is 159 s, while the average total computation time required to solve the linear LEMPC optimization problem is 23.6 s (the nonlinear LEMPC average computation time is 560% more).

Other approaches to identify the empirical model could be used. To demonstrate this, several other methods were used to obtain a linear model of Eq. 54 and similar one operating period (1 h) simulations were performed. Specifically, a model was obtained through the following methods: least squares parameter fit using the input/output data obtained through step tests, Jacobian linearization of the nonlinear model of Eq. 54 around the steady-state, applying the MOESP algorithm to input/output data generated from sinusoidal input response, and applying the MOESP algorithm to

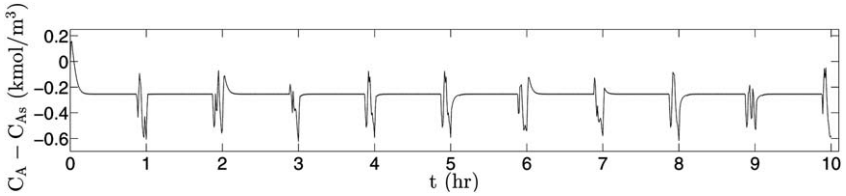

Figure 7. Closed-loop state trajectory ($x_1 = C_A - C_{As}$) of the CSTR under the linear LEMPC over 10 h.

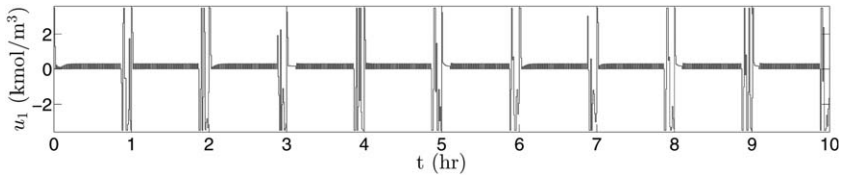

Figure 8. Input trajectory ($u_1 = C_{A0} - C_{A0s}$) under the linear LEMPC over 10 h.

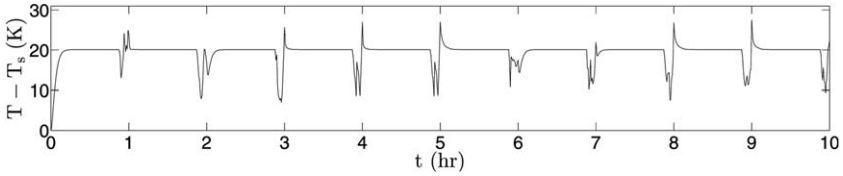

Figure 9. Closed-loop state trajectory ($x_2 = T - T_s$) of the CSTR under the linear LEMPC over 10 h.

input/output data generated from impulse input response. The closed-loop average economic performance of these simulations are reported in Table 2. From Table 2, similar closed-loop performance was achieved in each case and in all cases, the closed-loop performance was better under LEMPC than that achieved by steady-state operation. The linear LEMPC using the model of Eq. 57 achieved the best performance by design (extensive closed-loop simulations under the LEMPC were employed to construct and validate the model of Eq. 57). In all cases, closed-loop stability (boundedness of the closed-loop state in $\Omega_{\hat{\rho}}$) was achieved.

Improved accuracy with empirical models

Given that the CSTR exhibits nonlinear dynamic behavior (Eq. 54), the empirical model can only accurately predict the behavior within a limited region of state-space. In the previous simulations, the linear LEMPC computed a different input trajectory compared to the nonlinear LEMPC at the end of each operating period owing to the fact that the linear model did not accurately predict the evolution within this region of operation (c.f., Figure 4). In this section, we consider two methods that improve the accuracy of the empirical model used in the LEMPC: employing on-line system identification and using multiple linear models to describe the process within different regions of operation.

The first method that is investigated is on-line system identification. In on-line system identification, the first model used in the linear LEMPC is the model of Eq. 57. The model is used for only one operating period. At the end of the operating period, the closed-loop input/output data of the first operating period are used to compute a new model from the MOESP algorithm. At the end of each subsequent operating period, a new model is generated via the input/output data of the previous operating period and is used in the LEMPC over the next operating period. Over the course of a 10-h simulation, the average economic cost with on-line system identification was 15.41. Recall, for the 10-h simulation under linear LEMPC without on-line system identification (Figures 7–10), the average economic cost was 15.29 and a less than 0.7% improvement in the closed-loop performance was realized with the on-line system identification. For this particular example, little benefit was achieved when using this on-line system identification technique.

The second method that is investigated is formulating and applying linear LEMPC with multiple linear models. In this method, multiple linear models are regressed off-line for different regions of operation. Given that employing multiple linear models can more accurately predict the behavior of the nonlinear CSTR, a larger estimate of the level sets used in the linear LEMPC can be used. For this set of simulations, the level sets used in the LEMPC design were $\hat{\rho}=368.0$ and $\hat{\rho}_e=340.0$. Operating the CSTR over a larger region in state space is desirable from a process economics standpoint given that the (instantaneous) production rate scales with the exponential of $-1/T$ (i.e., the production rate is larger at higher temperatures). When multiple linear models were used within the linear LEMPC, the model used in the LEMPC optimization problem was selected on the basis of which region the initial condition was in. After extensive simulations, three models were identified for three regions in state-space. The first model is

$$A=\begin{bmatrix} -34.5 & -0.473 \\ 1430 & 18.1 \end{bmatrix},\ B=\begin{bmatrix} 5.24 & -8.09\times10^{-6} \\ -11.6 & 4.57\times10^{-3} \end{bmatrix} \quad (62)$$

and is most accurate for deviation temperatures less than 35.0 K (i.e., $x_2 \leq 35.0$). The second model is

$$A=\begin{bmatrix} -48.6 & -0.657 \\ 1960 & 23.2 \end{bmatrix},\ B=\begin{bmatrix} 6.22 & -1.13\times10^{-5} \\ 189 & 8.98\times10^{-3} \end{bmatrix} \quad (63)$$

and is most accurate for deviation temperatures between 35.0 and 43.0 K. The third model is

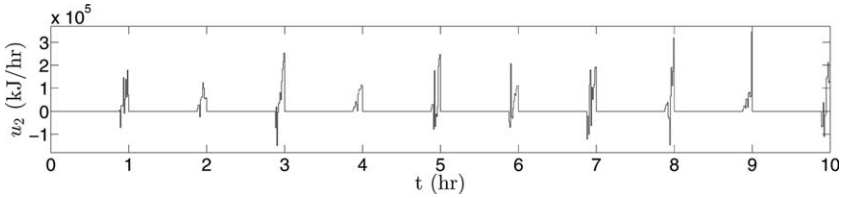

Figure 10. Input trajectory ($u_2 = Q - Q_s$) under the linear LEMPC over 10 h.

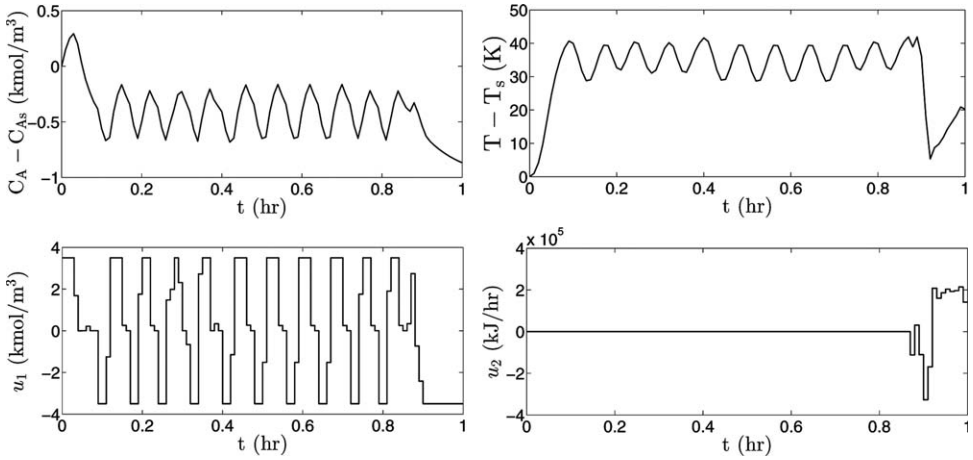

Figure 11. The closed-loop trajectories of the CSTR under the linear LEMPC (linear model of Eq. 62).

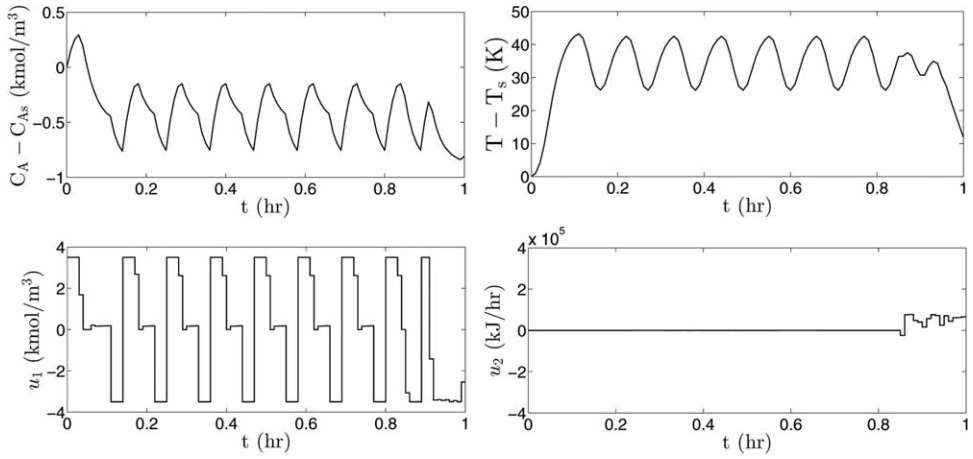

Figure 12. The closed-loop trajectories of the CSTR under the linear multiple-model LEMPC with two linear models.

$$A=\begin{bmatrix} 1.38 & 0.0894 \\ -476 & -10.7 \end{bmatrix},\ B=\begin{bmatrix} 0.901 & -1.24\times10^{-4} \\ 504 & 9.98\times10^{-3} \end{bmatrix} \quad (64)$$

and is most accurate for deviation temperatures greater than 43.0 K. The use of one, two, and three linear empirical models in the linear LEMPC was considered. Also, the nonlinear LEMPC was also considered for comparison purposes. The linear LEMPC based on one model uses the model of Eq. 62, the linear multiple-model LEMPC based on two models uses the models of Eqs. 62 and 63, and the linear multiple-

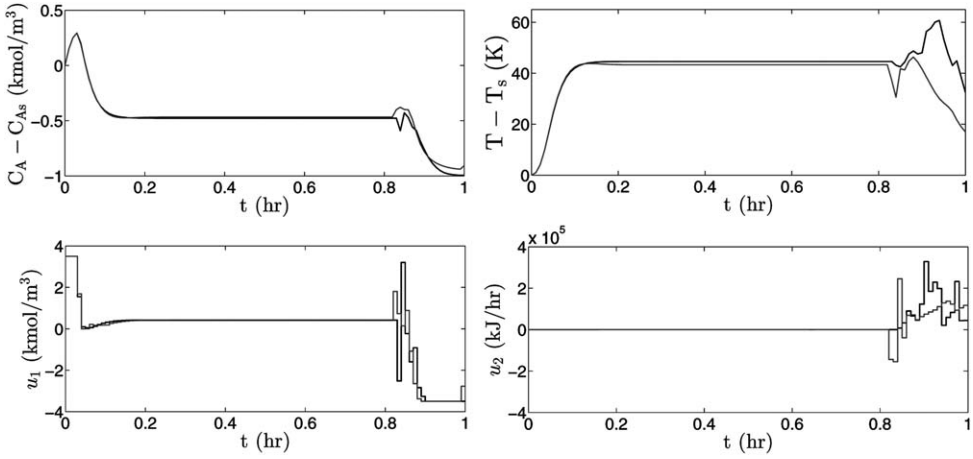

Figure 13. The closed-loop trajectories of the CSTR under the linear multiple-model LEMPC with three linear models (gray line) and under the nonlinear LEMPC (black line).

Table 2. Average Economic Cost (J_e) for One Period of Operation (1 h) Using Various Modeling Methods

Model	J_e
Nonlinear model	15.77
Linear model of Eq. 57	15.70
Least squares model	15.48
Jacobian linearization of nonlinear model	15.39
Sinusoidal system ID	15.39
Impulse system ID	15.51

model LEMPC based on three models uses the models of Eqs. 62–64.

One operating period simulations were completed with each LEMPC. The closed-loop trajectories for the CSTR under the linear LEMPC with one model, under the linear multiple-model LEMPC with two models, and under the linear multiple-model LEMPC with three models and under the nonlinear LEMPC are shown in Figures 11–13, respectively. From these figures, the closed-loop evolution of the CSTR under the linear LEMPC with one and two models is much different than that under the linear multiple-model LEMPC with three models and the nonlinear LEMPC because the CSTR under LEMPC is initially driven to and maintained in a region where the first and second models are not accurate. The closed-loop behavior of the CSTR under the linear multiple-model LEMPC with three models and the nonlinear LEMPC is similar, with the most significant deviation being observed toward the end of the operation period (Figure 14). The closed-loop average economic costs for these simulations are given in Table 3 and demonstrate that increasing the number of linear models used in the LEMPC improves the closed-loop performance and extends the region of time-varying operation (c.f., in Figures 4 and 14). Over the 1-h length of operation, the total computation time under the nonlinear LEMPC is 205.2 s and under the linear LEMPC

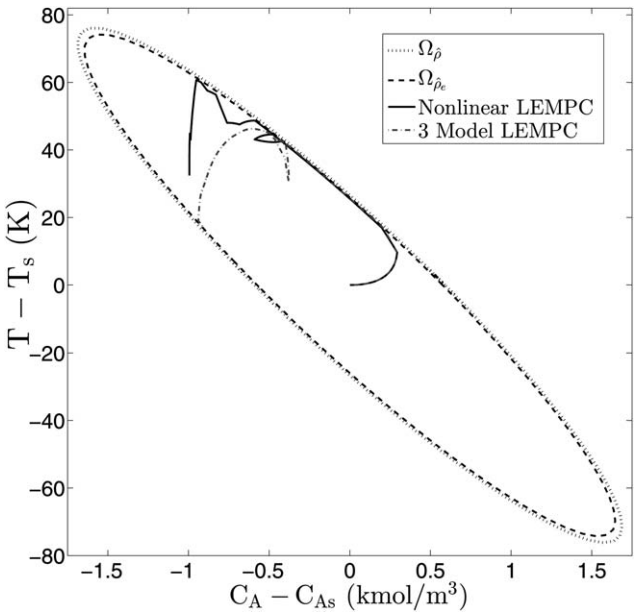

Figure 14. The closed-loop state trajectories of the CSTR under the linear multiple-model LEMPC with three linear models (dashed-dotted line) and under the nonlinear LEMPC (solid line).

Table 3. Average Economic Cost for the CSTR Under LEMPC Formulated with Multiple Empirical Models as Well as with the Nonlinear Model for One Period of Operation (1 h)

Method	J_e
One linear model	16.61
Two linear models	16.80
Three linear models	17.14
Nonlinear Model	17.22

with three empirical models is 20.4 s (the computation time for the nonlinear LEMPC is 906% greater than the computation time for the linear LEMPC with three empirical models).

Conclusions

In this work, an LEMPC method formulated with empirical models was considered for nonlinear process systems. Under the assumption that there is a sufficiently small error between the empirical linear model and the one of the linearization of the nonlinear model at the steady-state around which time-varying operation is considered, sufficient conditions such that the LEMPC formulated with the empirical linear model will guarantee closed-loop stability of the nonlinear system in the sense of boundedness of the closed-loop state in a compact set were derived. A chemical process example demonstrated the application of the proposed method and extensive simulation results were given. From these results, a similar closed-loop behavior between the chemical process under the LEMPC with the nonlinear model and under the LEMPC with an empirical model was observed with comparable closed-loop economic performance. However, a significant decrease in the computation time required to solve the LEMPC with a linear model compared to LEMPC with a nonlinear model was observed. In all of the simulations, the LEMPC with the linear model maintained closed-loop stability and obtained better closed-loop economic performance than that obtained at steady-state.

Acknowledgment

Financial support from the National Science Foundation and the Department of Energy is gratefully acknowledged.

Literature Cited

1. Engell S. Feedback control for optimal process operation. *J Process Control*. 2007;17:203–219.
2. Angeli D, Amrit R, Rawlings JB. On average performance and stability of economic model predictive control. *IEEE Trans Automat. Contr*. 2012;57:1615–1626.
3. Heidarinejad M, Liu J, Christofides PD. Economic model predictive control of nonlinear process systems using Lyapunov techniques. *AIChE J*. 2012;58:855–870.
4. Huang R, Harinath E, Biegler LT. Lyapunov stability of economically oriented NMPC for cyclic processes. *J Process Control*. 2011; 21:501–509.
5. Ellis M, Durand H, Christofides, PD. A tutorial review of economic model predictive control methods. *J Process Control*. 2014;24:1156–1178.
6. Ellis M, Christofides, PD. On finite-time and infinite-time cost improvement of economic model predictive control for nonlinear systems. *Automatica*. 2014;50:2561–2569.
7. Grüne L, Stieler M. Asymptotic stability and transient optimality of economic MPC without terminal conditions. *J. Process Control*. 2014;24:1187–1196.

8. Müller MA, Angeli D, Allgöwer F. On the performance of economic model predictive control with self-tuning terminal cost. *J. Process Control*. 2014;24:1179–1186.
9. Ogunnaike BA, Ray WH. *Process Dynamics, Modeling, and Control*. New York: Oxford University Press, 1994.
10. Åström KJ, Eykhoff P. System identification: a survey. *Automatica*. 1971;7:123–162.
11. Ljung L. *System Identification: Theory for the User*. Upper Saddle River, NJ: Prentice Hall, 1999.
12. Pearson RK. Selecting nonlinear model structures for computer control. *J Process Control*. 2003;13:1–26.
13. Doyle FJ, Pearson RK, and Ogunnaike BA. *Identification and Control Using Volterra Models*. Springer, 2002.
14. Billings SA. *Nonlinear System Identification: NARMAX Methods in the Time, Frequency, and Spatio-Temporal Domains*. John Wiley, 2013.
15. Murray-Smith R, Johansen T. *Multiple Model Approaches to Nonlinear Modelling and Control*. CRC press, 1997.
16. Jin X, Huang B, Shook DS. Multiple model LPV approach to nonlinear process identification with EM algorithm. *J Process Control*. 2011;21:182–193.
17. Hariprasad K, Bhartiya S, Gudi RD. A gap metric based multiple model approach for nonlinear switched systems. *J Process Control*. 2012;22:1743–1754.
18. Fruzzetti KP, Palazoğlu A, McDonald KA. Nonlinear model predictive control using Hammerstein models. *J Process Control*. 1997;7: 31–41.
19. Norquay SJ, Palazoğlu A, Romagnoli JA. Model predictive control based on Wiener models. *Chem Eng Sci*. 1998;53:75–84.
20. Bloemen HHJ, Van Den Boom TJJ, Verbruggen HB. Model-based predictive control for Hammerstein-Wiener systems. *Int J Control*. 2001;74:482–495.
21. Aumi S, Mhaskar P. Integrating data-based modeling and nonlinear control tools for batch process control. *AIChE J*. 2012;58:2105–2119.
22. Yu C, Roy RJ, Kaufman H, Bequette BW. Multiple-model adaptive predictive control of mean arterial pressure and cardiac output. *IEEE Trans. Biomed Eng*. 1992;39:765–778.
23. Verhaegen M, Deprettere E. A fast, recursive MIMO state space model identification algorithm. In: *Proceedings of the 30th IEEE Conference on Decision and Control*, Brighton, UK, 1991:1349–1354.
24. Verhaegen M, Dewilde P. Subspace model identification Part 1. The output-error state-space model identification class of algorithms. *Int J Control*. 1992;56:1187–1210.
25. Van Overschee P, De Moor B. N4SID: subspace algorithms for the identification of combined deterministic-stochastic systems. *Automatica*. 1994;30:75–93.
26. Viberg M. Subspace-based methods for the identification of linear time-invariant systems. *Automatica*. 1995;31:1835–1851.
27. Qin SJ. An overview of subspace identification. *Comput Chem Eng*. 2006;30:1502–1513.
28. Huang B, Kadali R. Dynamic modeling, predictive control and performance monitoring. London: Springer, 2008.
29. Van Overschee P, De Moor B. *Subspace Identification for Linear Systems: Theory, Implementation, Application*. Boston, MA: Kluwer Academic Publishers, 1996.
30. Chou CT, Verheagen M. Subspace algorithms for the identification of multivariable dynamic errors-in-variables models. *Automatica*. 1997;33:1857–1869.
31. Favoreel W, De Moor B, Van Overschee P. Subspace state space system identification for industrial processes. *J Process Control*. 2000;10:149–155.
32. Larimore WE. Canonical variate analysis in identification, filtering, and adaptive control. In *Proceedings of the 29th IEEE Conference on Decision and Control*, vol. 2, 1990:596–604.
33. Verhaegen M. Identification of the deterministic part of MIMO state space models given in innovations form from input-output data. *Automatica*. 1994;30:61–74.
34. Markovsky I, Willems JC, Rapisarda P, De Moor BLM. Algorithms for deterministic balanced subspace identification. *Automatica*. 2005; 41:755–766.
35. Anderson SR, Kadirkamanathan V. Modelling and identification of non-linear deterministic systems in the delta-domain. *Automatica*. 2007;43:1859–1868.
36. Massera JL. Contributions to stability theory. *Ann Math*. 1956;64: 182–206.
37. Khalil HK. *Nonlinear Systems*, 3rd ed. Upper Saddle River, NJ: Prentice Hall, 2002.
38. Lin Y, Sontag ED. A universal formula for stabilization with bounded controls. *Syst Contr Lett*. 1991;16:393–397.
39. Kokotović P, Arcak M. Constructive nonlinear control: a historical perspective. *Automatica*. 2001;37:637–662.
40. El-Farra NH, Christofides PD. Bounded robust control of constrained multivariable nonlinear processes. *Chem Eng Sci*. 2003;58:3025–3047.
41. Christofides PD, El-Farra NH. *Control of Nonlinear and Hybrid Process Systems: Designs for Uncertainty, Constraints and Time-Delays*. Berlin, Germany: Springer-Verlag, 2005.
42. Muñoz de la Peña D, Christofides PD. Lyapunov-based model predictive control of nonlinear systems subject to data losses. *IEEE Trans Automat Contr*. 2008;53:2076–2089.
43. Ellis M, Karafyllis I, Christofides PD. Stabilization of nonlinear sampled-data systems and economic model predictive control application. In: *Proceedings of the American Control Conference*, Portland, OR, 2014:5594–5601.
44. Sontag ED. A 'universal' construction of Artstein's theorem on nonlinear stabilization. *Syst Contr Lett*. 1989;13:117–123.
45. Wächter A, Biegler LT. On the implementation of an interior-point filter line-search algorithm for large-scale nonlinear programming. *Math Program*. 2006;106:25–57.

Manuscript received Sep. 14, 2014, and revision received Nov. 2, 2014.